# Determination of full piezoelectric complex parameters using gradient-based optimization algorithm

**C Y Kiyono[1], N Pérez[2], E C N Silva[1]**

[1] Department of Mechatronics and Mechanical Systems Engineering, Escola Politécnica, Universidade de São Paulo, Brazil

[2] Centro Universitário de Paysandú, Universidad de la República, Uruguay

E-mail: ckiyono@usp.br

April 2015

**Abstract.** At present, numerical techniques allow the precision simulation of mechanical structures. However the results are limited by the knowledge of the material properties. In the case of piezoelectric ceramics, the full model determination in the linear range involves five elastic, three piezoelectric, and two dielectric complex parameters. A successful solution to obtain piezoceramic properties consists in comparing the experimental measurement of the impedance curve and the results of a numerical model by using the Finite Element Method (FEM). Previous works have proposed very complicated methods highly dependent on user interaction and expertise with piezoelectric materials. In this work, a new systematic and efficient optimization method is proposed to adjust the full piezoelectric complex parameters in the FEM model. The only information required from the user is the experimental data (impedance and phase data acquired by an impedometer), the geometry, and initial values for the properties. The highlight of this method is the combination of a FEM routine implemented using an 8-noded axisymmetric element with a gradient-based optimization routine based on the Method of Moving Asymptotes (MMA). The main objective of the optimization procedure is to minimize the quadratic difference between the experimental and numerical electrical conductance and resistance curves (to consider resonance and anti-resonance frequencies). To assure the convergence of the optimization procedure, this work proposes restarting the optimization loop whenever the solution gets trapped in an undesired local minima or ends in an unfeasible solution. An experimental example using a PZ27 sample is presented showing that the numerical model can be accurately adjusted to the experimental curves.

## 1. Introduction

In most of the studies involving CAE (Computer Aided Engineering) simulations and experimental characterization of piezoelectric elements, it is very common to face the fact that the material properties provided by the supplier are not accurate. Figure 1 presents

the electrical impedance curves obtained experimentally, by using an impedometer, and numerically, by using the FEM with the material properties provided by the manufacturer in the case of a PZ27 piezoelectric ceramic form Ferroperm [1]. In this case, damping has not been considered in the numerical modeling. A great difference between the curves can be noticed, which can compromise all the numerical modeling, and hence, the validation of the numerical and experimental results.

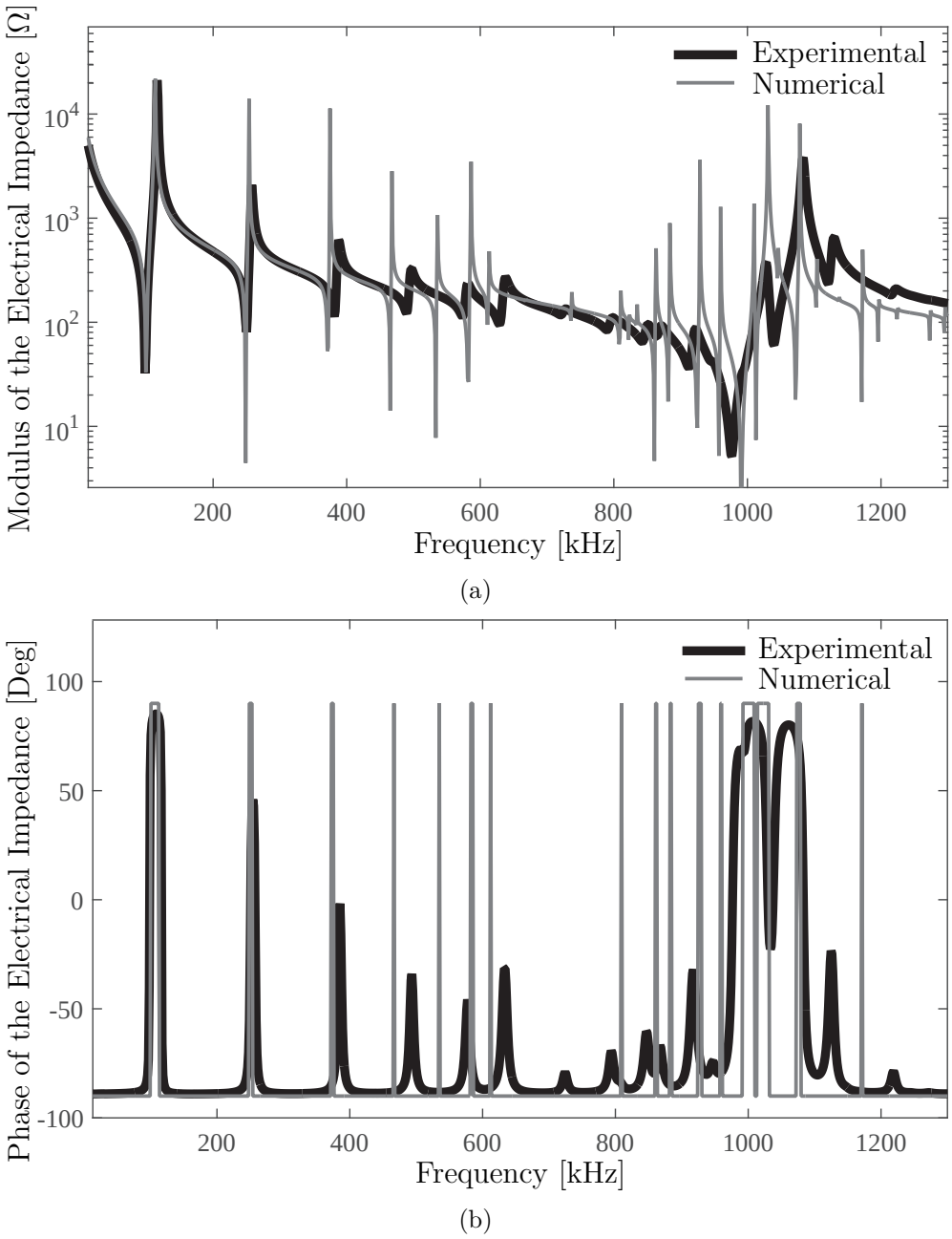


**Figure 1.** Comparative example between the electrical impedance curves obtained experimentally (thick black line) and numerically (thin gray line) with the material properties provided by the supplier, for the PZ27 (diameter = 10 mm and thickness = 2 mm). Numerical simulation without damping.

The piezoelectric material properties characterization has been extensively studied in literature [2–6]. In order to obtain the piezoelectric material properties, the piezoceramics are cut in particular shapes that decouples the resonance modes allowing an analytical solution. The most accepted methodology to obtain these properties is described in the IEEE Standard on Piezoelectricity [7], however this traditional methodology is very complex and requires samples with specific geometries and measuring the mechanical deformations and electrical field. In another approach, some works have implemented an optimization strategy in order to minimize the difference between numerical and experimental electrical impedance curves. The first works using that approach [8, 9] treated the problem for a narrow frequency range, which can result in inaccurate property values.

In a similar approach, Pérez et. al [10] presented a characterization method considering a wide frequency range. They propose two steps to obtain the real piezoelectric properties. In the preliminary step, the sensitivity of the resonance frequencies are calculated with respect to the material properties. These sensitivities are graphically post-processed and the user must choose which frequencies should be used to optimize some properties. Thus, a preliminary solution is obtained that approximates the numerical electrical conductance and resistance curves to the experimental curves. In the refinement step, an optimization algorithm based on the Nelder-Mead simplex method is used to refine the solution and tune the remaining real properties. However, this optimization routine does not use the objective function sensitivity, being very susceptible to local minima. This method, although it is very robust and accurate, depends heavily on user interaction and his expertise with piezoelectric materials.

Another drawback is that the IEEE standard assumes a lossless material and several numeric works model the damping by using the Rayleigh coefficients. Thus, they obtain only the real values for the elastic, dielectric and piezoelectric parameters. It is well known, since the sixties, that the losses in the piezoelectric model can be introduced by using complex numbers in the piezoelectric constitutive equations [11]. The identification of the complex model has been addressed by several researchers in the last years showing the importance of the imaginary part to take into account the losses [12, 13].

Recently, Pérez [14] have extended their work to the imaginary properties of the piezoelectric material, also considering a wide frequency range. They have used the same method proposed on [10] to obtain the full piezoelectric complex properties, however, they first obtain the real properties and later the imaginary properties, separately. This procedure is also susceptible to local minima since the imaginary property values depend on the real property values. In addition, they have implemented an in-house FEM software in Matlab that allows the modeling of piezoelectric structures with complex properties, which is not possible in most commercial FEM softwares. The finite element implemented by them is the 4-noded axisymmetric isoparametric piezoelectric 2D solid element, which can model only discs and rings structures. This element is very simple to implement, however, in order to model the structure accurately, the mesh need to

be well refined, and the recommended number of elements depends on the wave-length. For instance, for a 20x2 mm (diameter x thickness) piezoceramic disc, the minimum recommended number of elements is equal to 4000 (200x20 elements) to model half of the axisymmetric section (see figure 2 for reference). In an iterative optimization procedure, for a wide frequency range, the FEM can be computationally inefficient. Although these mentioned issues, the results presented in their work show that the numerical curves (modulus and phase of the electrical impedance) are practically equal to the experimental curves for the obtained full piezoelectric complex properties. Again, although robust and accurate, this method requires too much user iteration and expertise.

This work proposes a similar approach for obtaining the full piezoelectric complex properties following the works mentioned before. However, the method described here is totally systematic and more efficient computationally. The real and imaginary parts of the complex piezoelectric properties are obtained simultaneously, minimizing the local minima problem and simplifying the process. A wide frequency range is also considered in order to obtain more accurate piezoelectric properties. The only information required from the user is the experimental data (impedance and phase data acquired by an impedometer), the mass density, the geometry of the piezoceramic disc (diameter and thickness), and the real part of the piezoelectric properties provided by the manufacturer, when available. The efficiency in the FEM computation presented in this work is improved (compared to [14]) by using the 8-noded axisymmetric isoparametric piezoelectric 2D plane element, which allows a significant reduction of the total number of elements in the FEM routine, when compared to the 4-noded element. In section 2.1 a convergence test is evaluated, which shows that the electrical response is accurately modeled by using only 250 elements (50x5 elements). This grid size reduction corresponds to a reduction of 83.6% of computational time in the same PC, when compared to the computational time of the 4-noded element for 200x20 mesh.

The objective of the current method is to minimize the difference between the electrical conductance and resistance curves obtained experimentally and numerically (by using FEM), similarly to [10, 14]. The real and imaginary piezoelectric properties are called here as design variables, which are iteratively updated by an optimization algorithm in order to achieve the proposed objective. A very important contribution of this work is the use of the MMA (Method of Moving Asymptotes) [15] to update the design variables. MMA is a very efficient and robust gradient-based optimization algorithm, commonly used for structural optimization. The advantage of a gradient-based optimization algorithm is that it can overcome most of the unwanted local minima and improve the convergence of the method by reducing the total number of iterations (when compared to non gradient-based optimization algorithms). Even though, local minima around the global optimum can compromise the obtention of a satisfactory solution. Also, during the evaluations of the method, it has been observed that the initial design variables play a very important role in the success of the method. Thus, to guarantee the convergence of the optimization problem, it is proposed to restart the

optimization loop whenever the solution gets trapped in an undesired local minima or ends in an unfeasible solution. To restart the optimization loop, some conditions are proposed, which are described in section 4. The restart approach is another contribution in this work, together with the combination of the MMA and the 8-noded element.

To validate the method, the full piezoelectric properties obtained in section 6 are used to build a numerical model to serve as a reference to the proposed method. The FEM mesh of the reference model is more refined than the model of the optimization method to avoid the "inverse crime". Then, it is demonstrated that the optimized properties converges closely to the reference properties. Finally. an application example by using a PZ27 sample is presented showing that the numerical and experimental curves are practically identical.

All the evaluations and optimizations presented in this work have been made in a PC with Intel core i7-3960X CPU, 64 GB of RAM memory, running on Windows 7 Pro x64. The hole method have been implemented in Matlab, and most part of the code is parallelized (with *parfor* and *parpool*) to take advantage of all cores available. Thus, all computational time presented in this work is based on this configuration.

This paper is organized as follows. Section 2 presents the piezoelectricity theory, the FEM modeling and formulation implemented in this work, and the calculation of the electrical characteristics of the piezoelectric material. Section 3 presents the objective function of the optimization formulation, the configuration of the MMA algorithm, the proposed optimization method, and the sensitivity analysis. Then, section 4 presents the restart approach together with the conditions proposed to restart the optimization loop. Section 5 presents the method validation by using a numerical model as reference, and section 6 presents the application example. Finally, section 7 presents some concluding remarks.

## 2. Piezoelectricity and FEM

For piezoelectric materials, the mechanical behavior (strains and stresses) can be related to the electric behavior (electric field and electric displacements) according to the following constitutive system of equations in Voigh notation [16]:

$$\boldsymbol{\sigma} = \mathbf{c}^E \boldsymbol{\varepsilon} - \mathbf{e}\mathbf{E} \tag{1}$$

$$\mathbf{D} = \mathbf{e}\boldsymbol{\varepsilon} + \boldsymbol{\epsilon}^S \mathbf{E} \tag{2}$$

where $\mathbf{c}^E$, $\mathbf{e}$, and $\boldsymbol{\epsilon}^S$ are the elastic, piezoelectric and dielectric property matrices, respectively. The superscripts $E$ and $S$ indicate that these properties were obtained at a constant electric field and constant strain, respectively. For piezoelectric ceramics belonging to the 6mm symmetry class and with polarization along the $z$ axis, the

complex property matrices are represented as follows [16]:

$$\mathbf{c}^E = \begin{bmatrix} c_{11}+i\bar{c}_{11} & c_{12}+i\bar{c}_{12} & c_{13}+i\bar{c}_{13} & 0 & 0 & 0 \\ c_{12}+i\bar{c}_{12} & c_{11}+i\bar{c}_{11} & c_{13}+i\bar{c}_{13} & 0 & 0 & 0 \\ c_{13}+i\bar{c}_{13} & c_{13}+i\bar{c}_{13} & c_{33}+i\bar{c}_{33} & 0 & 0 & 0 \\ 0 & 0 & 0 & c_{44}+i\bar{c}_{44} & 0 & 0 \\ 0 & 0 & 0 & 0 & c_{44}+i\bar{c}_{44} & 0 \\ 0 & 0 & 0 & 0 & 0 & c_{66}+i\bar{c}_{66} \end{bmatrix} \tag{3}$$

$$\mathbf{e} = \begin{bmatrix} 0 & 0 & 0 & 0 & e_{15}+i\bar{e}_{15} & 0 \\ 0 & 0 & 0 & e_{15}+i\bar{e}_{15} & 0 & 0 \\ e_{31}+i\bar{e}_{31} & e_{31}+i\bar{e}_{31} & e_{33}+i\bar{e}_{33} & 0 & 0 & 0 \end{bmatrix} \tag{4}$$

$$\boldsymbol{\epsilon}^S = \begin{bmatrix} \epsilon_{11}+i\bar{\epsilon}_{11} & 0 & 0 \\ 0 & \epsilon_{11}+i\bar{\epsilon}_{11} & 0 \\ 0 & 0 & \epsilon_{33}+i\bar{\epsilon}_{33} \end{bmatrix} \tag{5}$$

where $c_{66} = (c_{11} + c_{12})/2$ and $\bar{c}_{66} = (\bar{c}_{11} + \bar{c}_{12})/2$. The imaginary properties are represented by an over bar, and the superscripts $E$ and $S$ are omitted to simplify the notation. Thus, there are 10 independent real properties and 10 independent imaginary properties, which are the design variables in this work. The real properties are related to the electro-mechanical response of the sample, that is, the resonance peaks positions in the impedance curve (see figure 1(a)), while the complex properties are related to the material damping, i.e., the energy losses that influence in the amplitude of the resonant modes.

### *2.1. FEM Modeling*

In this work, the 8-noded axisymmetric isoparametric piezoelectric 2D plane element is used to model ceramic discs. Figure 2 presents the piezoelectric disc, its equivalent FEM model, and a representation of the element. The 8-noded element is more accurate and efficient, i.e., the FEM model converges using fewer elements, and thus, reducing the computational cost. The mesh convergence test is presented in section 2.4. Because of symmetry, it is possible to consider only a quarter of the disc section. The suitably boundary conditions for the electric potential and displacement are shown in figure 2(b). The electric potential applied to the reduced axisymmetric model must be half of the electric potential applied to the complete disc model.

Thus, by assuming axisymmetric model, the property matrices of (3), (4), and (5) can be simplified as:

$$\mathbf{c} = \begin{bmatrix} c_{11}+i\bar{c}_{11} & c_{12}+i\bar{c}_{12} & c_{13}+i\bar{c}_{13} & 0 \\ c_{12}+i\bar{c}_{12} & c_{11}+i\bar{c}_{11} & c_{13}+i\bar{c}_{13} & 0 \\ c_{13}+i\bar{c}_{13} & c_{13}+i\bar{c}_{13} & c_{33}+i\bar{c}_{33} & 0 \\ 0 & 0 & 0 & c_{44}+i\bar{c}_{44} \end{bmatrix} \tag{6}$$

$$\mathbf{e} = \begin{bmatrix} 0 & 0 & 0 & e_{15}+i\bar{e}_{15} \\ e_{31}+i\bar{e}_{31} & e_{31}+i\bar{e}_{31} & e_{33}+i\bar{e}_{33} & 0 \end{bmatrix} \tag{7}$$

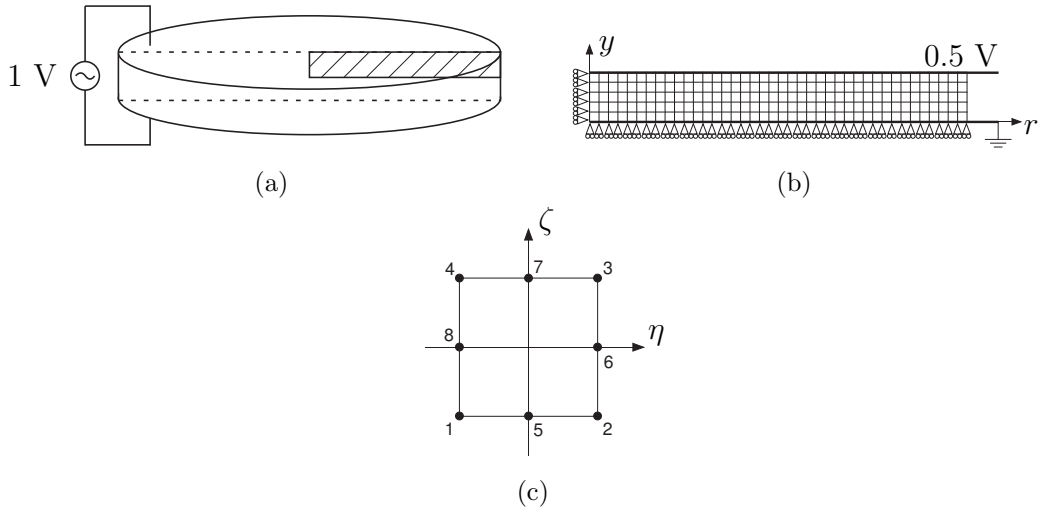


**Figure 2.** Representation of the piezoelectric disc, its equivalent FEM model, and the axisymmetric 2D element.

$$\boldsymbol{\epsilon}^S = \begin{bmatrix} \epsilon_{11} + i\bar{\epsilon}_{11} & 0 \\ 0 & \epsilon_{33} + i\bar{\epsilon}_{33} \end{bmatrix} \tag{8}$$

and still, the 20 independent (real+complex) properties are present in these matrices.

### *2.2. FEM Formulation*

The equilibrium equation system for the harmonic linear behavior is given by [17]:

$$\begin{bmatrix} -\omega^2\mathbf{M_{uu}} + \mathbf{K_{uu}} & \mathbf{K_{u\phi}} \\ \mathbf{K_{u\phi}}^T & \mathbf{K_{\phi\phi}} \end{bmatrix} \begin{Bmatrix} \mathbf{U} \\ \mathbf{\Phi} \end{Bmatrix} = \begin{Bmatrix} \mathbf{F} \\ \mathbf{Q} \end{Bmatrix} \tag{9}$$

where $\omega = 2\pi f$ and $f$ is the working frequency, $\mathbf{U}$, $\mathbf{\Phi}$, $\mathbf{F}$, and $\mathbf{Q}$ are the global vectors of mechanical displacements, electric potential, mechanical force, and electrical charge, respectively. $\mathbf{M_{uu}}$ is the mass global matrix and $\mathbf{K_{uu}}$, $\mathbf{K_{u\phi}}$, and $\mathbf{K_{\phi\phi}}$ are the global matrices of elastic, piezoelectric, and dielectric stiffness, respectively. The superscript $T$ indicates the transpose matrix, however it must not be confused with the conjugated transpose, because these matrices have complex values. These global matrices can be properly built by using the local element matrices, which for the piezoelectric axisymmetric 2D element are given by:

$$\mathbf{M_{uu}}^e = 2\pi\rho \int_{-1}^{1}\int_{-1}^{1} \mathbf{N_u}^T \mathbf{N_u} r |\mathbf{J}| d\eta d\xi \tag{10}$$

$$\mathbf{K_{uu}}^e = 2\pi \int_{-1}^{1}\int_{-1}^{1} \mathbf{B_u}^T \mathbf{c} \mathbf{B_u} r |\mathbf{J}| d\eta d\xi \tag{11}$$

$$\mathbf{K}^e_{\mathbf{u}\phi} = 2\pi \int_{-1}^{1}\int_{-1}^{1} \mathbf{B_u}^T \mathbf{e} \mathbf{B}_\phi r |\mathbf{J}| d\eta d\xi \tag{12}$$

$$\mathbf{K}^e_{\phi\phi} = 2\pi \int_{-1}^{1}\int_{-1}^{1} \mathbf{B}_\phi^T \boldsymbol{\epsilon} \mathbf{B}_\phi r |\mathbf{J}| d\eta d\xi \tag{13}$$

$$\tag{14}$$

where $\mathbf{c}$, $\mathbf{e}$, and $\boldsymbol{\epsilon}$ are given by (6), (7), and (8), respectively, $\rho$ is the material density, $r$ is the distance from the point in question to the axisymmetric axis (see figure 2(b)), given by:

$$r = \sum_{k=1}^{8} r_k N_k \tag{15}$$

The matrices $\mathbf{N_u}$, $\mathbf{B_u}$, and $\mathbf{B}_\phi$ are given by:

$$\mathbf{N_u} = \begin{bmatrix} N_1 & \cdots & N_8 & 0 & \cdots & 0 \\ 0 & \cdots & 0 & N_1 & \cdots & N_8 \end{bmatrix} = \begin{bmatrix} \mathbf{N} & \mathbf{0} \\ \mathbf{0} & \mathbf{N} \end{bmatrix} \tag{16}$$

$$\mathbf{B_u} = \begin{bmatrix} \frac{\partial \mathbf{N}}{\partial r} & \mathbf{0} \\ \mathbf{0} & \frac{\partial \mathbf{N}}{\partial z} \\ \frac{1}{r} & \mathbf{0} \\ \frac{\partial \mathbf{N}}{\partial r} & \frac{\partial \mathbf{N}}{\partial z} \end{bmatrix} \tag{17}$$

$$\mathbf{B}_\phi = \begin{bmatrix} \frac{\partial \mathbf{N}}{\partial r} \\ \frac{\partial \mathbf{N}}{\partial z} \end{bmatrix} \tag{18}$$

### *2.3. Calculation of Electrical Characteristics*

Before calculating the electrical characteristics of the model, such as impedance, conductance and resistance, the equilibrium system of (9) must be solved. In the experimental determination of the electrical impedance, a sinusoidal electric potential is applied at the piezoceramic electrodes, see figure 2. To have the same boundary conditions in the numerical model, the electrical degrees of freedom in the numerical model must be prescribed. To facilitate the understanding of the solution of (9) with prescribed (applied) electric potential, the electrical degrees of freedom are separated into electrode 1 ($\phi_{e1}$), electrode 2 ($\phi_{e2}$), and free ($\phi_f$), as represented in Figure 4, and $\boldsymbol{\phi}_{e1}$, $\boldsymbol{\phi}_{e2}$, and $\boldsymbol{\phi}_f$ are the electric potential vectors associated to these degrees of freedom.

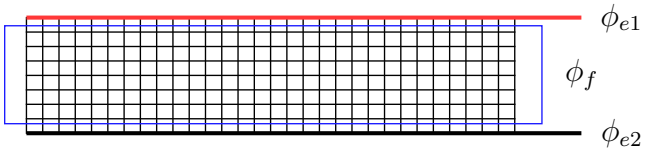


**Figure 3.** Electrical degrees of freedom.

Thus, by considering that the bottom electrode ($\phi_{e2}$) is grounded, and hence $\boldsymbol{\phi}_{e2} = \mathbf{0}$, it is possible to rewrite (9) in the following manner:

$$\begin{bmatrix} -\omega^2 \mathbf{M_{uu}} + \mathbf{K_{uu}} & \mathbf{K}_{\mathbf{u}\phi_f} & \mathbf{K}_{\mathbf{u}\phi_{e1}} \\ \mathbf{K}^T_{\mathbf{u}\phi_f} & \mathbf{K}_{\phi_f\phi_f} & \mathbf{K}_{\phi_f\phi_{e1}} \\ \mathbf{K}^T_{\mathbf{u}\phi_{e1}} & \mathbf{K}^T_{\phi_f\phi_{e1}} & \mathbf{K}_{\phi_{e1}\phi_{e1}} \end{bmatrix} \begin{Bmatrix} \mathbf{U} \\ \mathbf{\Phi}_f \\ \mathbf{\Phi}_{e1} \end{Bmatrix} = \begin{Bmatrix} \mathbf{F} \\ \mathbf{Q}_f \\ \mathbf{Q}_{e1} \end{Bmatrix} \tag{19}$$

Considering that $\mathbf{\Phi}_{e1}$ is known (applied electric potential for each node at the electrode surface), that there is no external loads being applied to the model ($\mathbf{F} = \mathbf{0}$), and that the internal electric charges are zero ($\mathbf{Q}_f = \mathbf{0}$), the unknown displacements $\mathbf{U}$

and electric potentials $\mathbf{\Phi}_f$ can be obtained by solving the following simplified system of equations:

$$\begin{bmatrix} -\omega^2\mathbf{M_{uu}} + \mathbf{K_{uu}} & \mathbf{K}_{\mathbf{u}\phi_f} \\ \mathbf{K}^T_{\mathbf{u}\phi_f} & \mathbf{K}_{\phi_f\phi_f} \end{bmatrix} \begin{Bmatrix} \mathbf{U} \\ \mathbf{\Phi}_f \end{Bmatrix} = \begin{bmatrix} \mathbf{K}_{\mathbf{u}\phi_{e1}} \\ \mathbf{K}_{\phi_f\phi_{e1}} \end{bmatrix} \mathbf{\Phi}_{e1} \tag{20}$$

Next, (19) is used to calculate the electrical charge for each node of the top electrode $\mathbf{Q}_{e1}$ as:

$$\mathbf{Q}_{e1} = [\, \mathbf{K}^T_{\mathbf{u}\phi_{e1}} \quad \mathbf{K}^T_{\phi_f\phi_{e1}} \quad \mathbf{K}_{\phi_{e1}\phi_{e1}} \,] \begin{Bmatrix} \mathbf{U} \\ \mathbf{\Phi}_f \\ \mathbf{\Phi}_{e1} \end{Bmatrix} \tag{21}$$

In the case of harmonic analysis, i.e., the electrical potential varies sinusoidal with angular frequency $\omega$, all magnitudes in the problem are also sinusoidal with the same frequency. From the electric charge, a vector containing the electric current flowing to each node $\mathbf{I}$ is calculated as:

$$\mathbf{I} = -i\omega\mathbf{Q}_{e1} \tag{22}$$

where $i$ represents the imaginary number. The physical electric current measured in the electrode wire is the sum of the electric current values of elements of $\mathbf{I}$. Thus, it is possible to calculate the electric impedance $Z$ and admittance $Y$:

$$Z = \mathbf{\Phi}^T_{e1}\mathbf{I} \tag{23}$$

$$Y = \frac{1}{Z} \tag{24}$$

Notice that $Z$ and $Y$ are complex numbers, the module of $Z$ is the ratio between the voltage and the current amplitudes whereas the phase of the complex number $Z$ represents the phase angle between both magnitudes. Finally, the electric conductance $G$ and resistance $R$ are calculated as:

$$G = Re\{Y\} \tag{25}$$

$$R = Re\{Z\} \tag{26}$$

where $Re$ means the real part. The importance of using $R$ and $G$ lays in the fact that maximum of $G$ curves occurs at resonant frequencies whereas the maximum of $R$ curves occurs at anti-resonant frequencies [10, 18]. Besides, $G$ is proportional to the electric power consumed by the sample, thus it is a representative magnitude that takes into account the energy losses.

Thus, we have the electrical characteristics of a numerical piezoelectric model. In the case of a real ceramic (experimental model), the sinusoidal response can be obtained by applying a sinusoidal voltage for each frequency or by using an impedometer. In either case the amplitude ($A$) and phase ($\theta$) of the electrical impedance are obtained. Assuming the phase angle expressed in degrees, the experimental electrical impedance can be calculated by:

$$Z = Ae^{i\theta\frac{\pi}{180}} \tag{27}$$

and the other characteristics ($Y$, $G$, and $R$) can be obtained by using (24), (25), and (26).

### *2.4. Mesh Convergence Test*

Figure 4 shows the conductance curves obtained by using different mesh discretizations: 20x2, 50x5, and 100x10 for the 8-noded element, and 100x10, 200x20, and 300x30 for the 4-noded element. The computing time for each mesh discretization is described in the legend of figure 4(a).

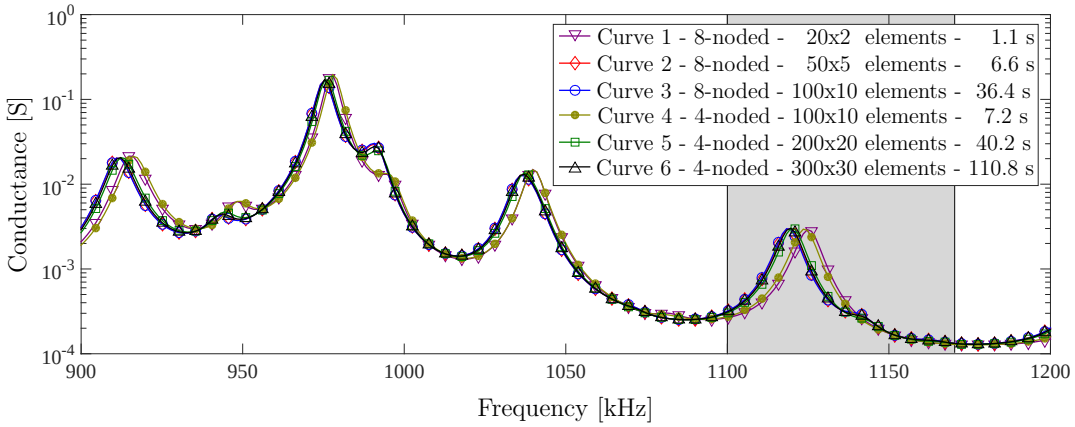


(a) 800 kHz to 1.3 MHz bandwidth.

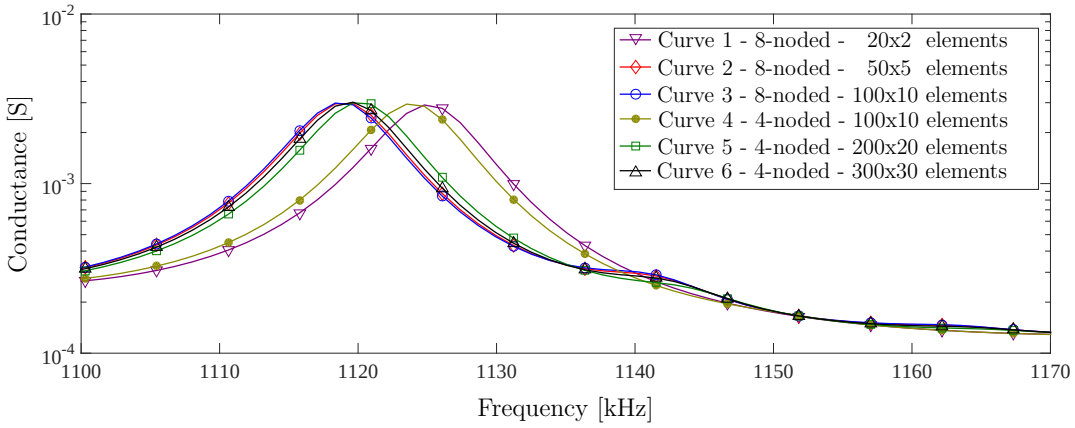


(b) Enlarged bandwidth from 1.1 MHz to 1.15 MHz.

**Figure 4.** Comparative graphs of the conductance curves for different mesh discretizations, using 4- and 8-noded elements. Figure (b) corresponds to the gray region of figure (a).

The piezoelectric complex properties used to build these graphs are described in table 1, and they correspond to the properties of the piezoelectric material PZ27 obtained by [14]. By analyzing the enlarged region (figure 4(b)), it can be noticed that curve 2 (8-noded element and 50x5 elements) is practically equal to curves 3 (8-noded element and 100x10 elements) and 6 (4-noded element and 300x30 elements). The processing time of these curves are equal to 6.6s, 36.4s, and 110.8s. This means that the 8-noded element with only 50x5 elements can accurately model the electrical behavior reducing the processing time about sixteen times (when compared to curve 6).

**Table 1.** Real and imaginary material properties for the Pz27, obtained by [14].

| | | | | | |
|---|---|---|---|---|---|
| $c_{11}$ | 118.1 | GPa | $\bar{c}_{11}$ | 0.56 | GPa |
| $c_{12}$ | 74.9 | GPa | $\bar{c}_{12}$ | 0.035 | GPa |
| $c_{13}$ | 73.8 | GPa | $\bar{c}_{13}$ | 0.024 | GPa |
| $c_{33}$ | 110.4 | GPa | $\bar{c}_{33}$ | 0.47 | GPa |
| $c_{44}$ | 20.27 | GPa | $\bar{c}_{44}$ | 0.36 | GPa |
| $e_{31}$ | -5.1 | C/m$^2$ | $\bar{e}_{31}$ | 0.0003 | C/m$^2$ |
| $e_{15}$ | 11.2 | C/m$^2$ | $\bar{e}_{15}$ | -0.039 | C/m$^2$ |
| $e_{33}$ | 16.0 | C/m$^2$ | $\bar{e}_{33}$ | -0.10 | C/m$^2$ |
| $\epsilon_{11}$ | 984 | $\times\epsilon_0$ | $\bar{\epsilon}_{11}$ | -0.06 | $\times\epsilon_0$ |
| $\epsilon_{33}$ | 830 | $\times\epsilon_0$ | $\bar{\epsilon}_{33}$ | -11 | $\times\epsilon_0$ |

$\epsilon_0 = 8.8541 \times 10^{-12}$ F/m and $\rho = 7707$ kg/m$^3$.

### *2.5. Alternative System of Units*

When working with piezoelectric materials, it is common to have a bad conditioned stiffness matrix because of the huge difference among the material property values. For instance, the elastic properties are given in GPa, and the dielectric properties are given in $10^{-12}$ F/m, or pF/m. This bad conditioning can generate numerical problems when solving the equilibrium equations and obtaining the electrical responses. To avoid that, this work applies the normalization of the material properties by changing the system of units from SI to an alternative system of units, presented in table 2.

**Table 2.** Conversion of the system of units.

| SI | Alternative |
|---|---|
| m (meters) | $10^3$ mm (mili meters) |
| V (Volt) | $10^{-6}$ MV (Mega Volt) |
| C (Coulomb) | $10^9$ nC (nano Coulomb) |
| Pa (Pascal) | $10^{-6}$ MPa (Mega Pascal) |
| kg (kilo grams) | $10^3$ g (grams) |
| A (Ampere) | $10^6$ $\mu$A (micro Ampere) |
| $\Omega$ (Ohm) | $10^{-12}$ T$\Omega$ (Tera Ohm) |
| Hz (Hertz) | $10^{-3}$ kHz (kilo Hertz) |
| F (Farad) | $10^{15}$ fF (femto Farad) |

## 3. Optimization Formulation

The main objective of this work is to obtain the full complex properties of piezoelectric materials. Essentially, the proposed objective function is to minimize the square difference between the electrical conductance and resistance curves, obtained

experimentally and numerically, by adjusting the piezoelectric complex properties of the numerical model.

However, one great concern in this project is the proper definition of the design variables values. They must be adequately scaled so that the sensitivity of the objective function with respect to them are well scaled. Otherwise, some variables can have higher priority than others in the optimization process, which means that some variables will be accurate and others will not. Thus, based on the properties obtained by [14] shown in table 1, by considering the alternative system of units, presented in table 2, and by proposing a scaling factor to properly scale the variables, it is proposed to define the design variables as described in table 3.

**Table 3.** Definition of the design variables.

| | | | | | |
|---|---|---|---|---|---|
| $c_{11}$ | $= x_1$ | $\times 10^4$ MPa | $\bar{c}_{11}$ | $= x_{11}$ | $\times 10^2$ MPa |
| $c_{12}$ | $= x_2$ | $\times 10^4$ MPa | $\bar{c}_{12}$ | $= x_{12}$ | $\times 10^2$ MPa |
| $c_{13}$ | $= x_3$ | $\times 10^4$ MPa | $\bar{c}_{13}$ | $= x_{13}$ | $\times 10^2$ MPa |
| $c_{33}$ | $= x_4$ | $\times 10^4$ MPa | $\bar{c}_{33}$ | $= x_{14}$ | $\times 10^2$ MPa |
| $c_{44}$ | $= x_5$ | $\times 10^4$ MPa | $\bar{c}_{44}$ | $= x_{15}$ | $\times 10^2$ MPa |
| $e_{31}$ | $= x_6$ | $\times 10^3$ nC/mm$^2$ | $\bar{e}_{31}$ | $= x_{16}$ | $\times 10^1$ nC/mm$^2$ |
| $e_{15}$ | $= x_7$ | $\times 10^3$ nC/mm$^2$ | $\bar{e}_{15}$ | $= x_{17}$ | $\times 10^1$ nC/mm$^2$ |
| $e_{33}$ | $= x_8$ | $\times 10^3$ nC/mm$^2$ | $\bar{e}_{33}$ | $= x_{18}$ | $\times 10^1$ nC/mm$^2$ |
| $\epsilon_{11}$ | $= x_9$ | $\times 10^2 \epsilon_0$ | $\bar{\epsilon}_{11}$ | $= x_{19}$ | $\times \epsilon_0$ |
| $\epsilon_{33}$ | $= x_{10}$ | $\times 10^2 \epsilon_0$ | $\bar{\epsilon}_{33}$ | $= x_{20}$ | $\times \epsilon_0$ |

$\epsilon_0 = 8.8541$ fF/mm and $\rho = 7707 \times 10^{-6}$ g/mm$^3$.

Then, $\mathbf{x}$ is defined as the design variables vector, such as:

$$\mathbf{x} = \{\, x_1 \quad x_2 \quad x_3 \quad x_4 \quad x_5 \quad x_6 \quad x_7 \quad x_8 \quad x_9 \quad x_{10} \quad \ldots \quad \ldots \quad x_{11} \quad x_{12} \quad x_{13} \quad x_{14} \quad x_{15} \quad x_{16} \quad x_{17} \quad x_{18} \quad x_{19} \quad x_{20} \,\} \tag{28}$$

Thus, the full piezoelectric complex properties are directly dependent on the design variables. The scaling factors have been established based on the results presented by [14]. This scaling may be different for other materials, and it can be modified to attend other specifications. Also, it is known that the piezoelectric property $e_{31}$ is always negative. Thus, its sign is included in the piezoelectric matrix property (7) so that $x_6$ is always positive.

Thus, based on the objective function proposed by [10], the objective function of this work is defined as:

$$\mathfrak{F}(\mathbf{x}) = \sum_{j=1}^{n_f} \left[\log_{10} G_j^{exp} - \log_{10} G_j^{num}(\mathbf{x})\right]^2 + \left[\log_{10} R_j^{exp} - \log_{10} R_j^{num}(\mathbf{x})\right]^2 \tag{29}$$

where the $\log_{10}$ function is used to equalize the conductance and resistance values in order to reduce the difference between the highest and the lowest resonant peaks.

$j = 1, \ldots, n_f$ is the frequency discretization, given a frequency range $f_{min} \leq f_j \leq f_{max}$, and $n_f$ is the number of frequencies used in the analysis.

The objective function can be written in matrix notation as:

$$\mathfrak{F}(\mathbf{x}) = \mathbf{L}^T \mathbf{H}(\mathbf{x}) \tag{30}$$

where

$$\mathbf{L} = \begin{bmatrix} 1 \\ \vdots \\ 1 \\ 1 \\ \vdots \\ 1 \end{bmatrix} \quad \text{and} \quad \mathbf{H}(\mathbf{x}) = \begin{bmatrix} H_1^2(\mathbf{x}) \\ \vdots \\ H_{n_f}^2(\mathbf{x}) \\ H_{n_f+1}^2(\mathbf{x}) \\ \vdots \\ H_{2n_f}^2(\mathbf{x}) \end{bmatrix} \tag{31}$$

where

$$H_k = \begin{cases} \log_{10} G_k^{exp} - \log_{10} G_k^{num}(\mathbf{x}) & \text{for } k = 1, \ldots, n_f \\ \log_{10} R_{k-n_f}^{exp} - \log_{10} R_{k-n_f}^{num}(\mathbf{x}) & \text{for } k = n_f + 1, \ldots, 2n_f \end{cases} \tag{32}$$

Thus, the optimization problem can be formulated the following manner:

$$\begin{aligned} &\underbrace{\text{Minimize}}_{\mathbf{x}} : \quad \mathfrak{F}(\mathbf{x}) = \mathbf{L}^T \mathbf{H}(\mathbf{x}) \\ &\text{subject to:} \quad \mathbf{x}^{min} \leq \mathbf{x} \leq \mathbf{x}^{max} \end{aligned} \tag{33}$$

where $\mathbf{x}^{min}$ and $\mathbf{x}^{max}$ are the minimum and maximum values for each variable. This is the problem solved iteratively by using the Method of Moving Asymptotes (MMA) [15].

### *3.1. MMA Optimization Algorithm*

The method of moving asymptotes is a gradient-based optimization algorithm written and kindly provided by Professor Kristen Svanberg [15]. It has been largely used because it is extremely efficient in handling a large number of variables and constraints. Also, it can be used for different kinds of applications.

The asymptotes are essentially the limits that the variables can assume at each iteration step of the optimization process. Two asymptotes for each variable $i$ are used during the optimization loop, the lower $a^l$ and the upper $a^u$ asymptotes. They are initially defined as $a_i^l = 0$ and $a_i^u = 1$, and they change between iterations following an intern rule of the MMA algorithm.

For minimization of least square problems by using the MMA algorithm, it is suggested to modify the optimization problem in the following manner [15]:

$$\begin{aligned} &\underbrace{\text{Minimize}}_{\mathbf{x}} : \\ &\text{subject to:} \quad H_k(\mathbf{x}) \leq 0, \qquad k = 1, ..., 2n_f \\ &\qquad\qquad\quad H_k(\mathbf{x}) \geq 0, \qquad k = 1, ..., 2n_f \\ &\qquad\qquad\quad \mathbf{x}^{min} \leq \mathbf{x} \leq \mathbf{x}^{max} \end{aligned} \tag{34}$$

It means that, instead of minimizing the summation of $H_k^2$, $H_k$ is used as a constraint in a problem without objective function. By doing that, the problem forces all $H_k$ to be lesser or equal to 0 and greater or equal to 0, which means that $H_k$ will be as close to 0 as possible. Thus, the following parameters must be configured as inputs to the MMA algorithm:

$$\begin{array}{lll} m & = 2n_f + 2n_f & \\ f_0 & = 0 & \\ f_k & = H_k & k = 1, ..., 2n_f \\ f_{n_f+k} & = -H_k & k = 1, ..., 2n_f \\ a_0 & = 1 & \\ a_l & = 0 & l = 1, ..., m \\ d_l & = 2 & l = 1, ..., m \\ c_l & = 0 & l = 1, ..., m \end{array} \tag{35}$$

where $m$ is total number of constraints, $f_0$ is the objective function value, and $f_k$ are the constraints. $a_0$, $a_l$, $d_l$, and $c_l$ are internal parameters of the MMA algorithm, which have different values depending on the optimization problem. However, the modification presented in (34) is applied only as input to the MMA algorithm. The objective function in (29), or (30), is still used to evaluate the convergence of the optimization process.

### *3.2. Proposed Method*

Comparing to previous works in this area, three major improvements can be highlighted in the present work. First, the optimization technique to obtain the full complex piezoelectric properties is totally systematic and highly robust, and because of the gradient based optimization algorithm MMA, this technique converges simultaneously both in the real and the imaginary part of the model. Second, the use of the 8-noded element FEM software allows the reduction of the simulation time and improves the accuracy of the FEM model. Third, the resulting optimization algorithm requires very few user interactions. The software only requires that the user provides the dimensions of the piezoelectric disc, the mass density, a file containing the experimental data, and the initial real properties of the piezoelectric material, which can be the properties provided by the manufacturer.

With the experimental data, the software initially computes the electrical conductance and resistance curves of the experimental model and saves this information. Next, the software builds the numerical model (by using FEM), computes the numerical electrical conductance and resistance curves, and then calculates the square difference between experimental and numerical curves by using the objective function of (29). The next step is to verify convergence of the optimization problem which is when the objective function becomes smaller than a specified tolerance. If convergence is achieved, then the full piezoelectric complex properties have been found. Otherwise, the software continues to the sensitivity analysis, and finally, updates the design variables by using the MMA algorithm. This process is repeated in an optimization loop until convergence is

achieved. This optimization procedure can be summarized into the flowchart presented in figure 5.

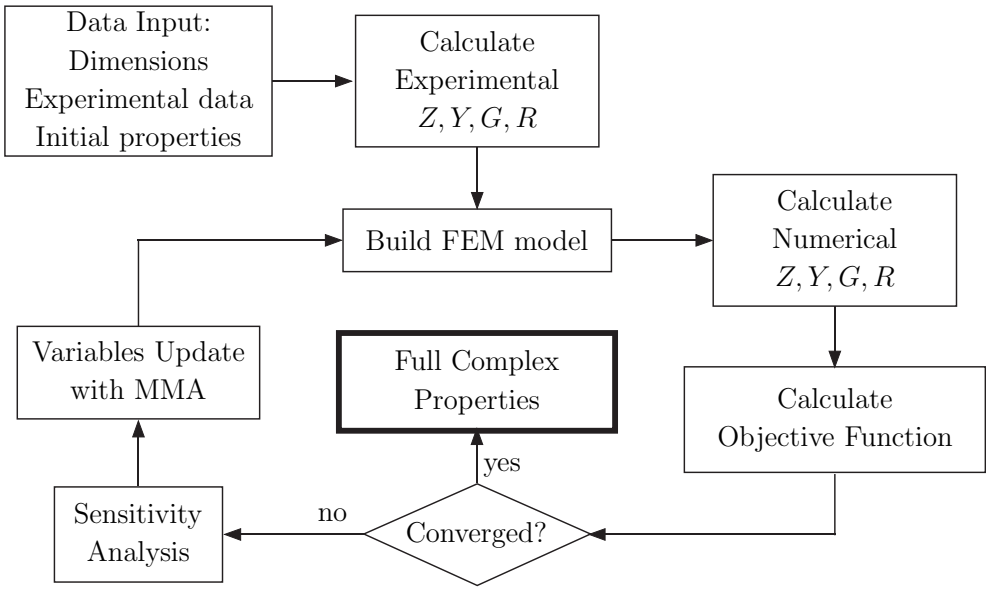


**Figure 5.** Flowchart of the optimization method proposed.

### *3.3. Sensitivity Analysis*

The MMA algorithm requires the derivatives of the objective function and constraints with respect to the design variables. In the modified optimization problem ((33)), only the differentiation of $H_k$ must be calculated as follows:

$$\frac{\partial H_k}{\partial x_i} = \begin{cases} \frac{-1}{G_k^{num} \ln 10} \frac{\partial G_k^{num}}{\partial x_i}, & \text{for } k = 1, ..., n_f \\ \\ \frac{-1}{R_{k-n_f}^{num} \ln 10} \frac{\partial R_{k-n_f}^{num}}{\partial x_i}, & \text{for } k = n_f + 1, ..., 2n_f \end{cases} \tag{36}$$

The differentiation of the electrical conductance (25) can be calculated as:

$$\frac{\partial G}{\partial x_i} = Re\left\{\frac{\partial Y}{\partial x_i}\right\} \tag{37}$$

where

$$\frac{\partial Y}{\partial x_i} = -\frac{1}{Z^2}\frac{\partial Z}{\partial x_i} \tag{38}$$

The differentiation of the electrical resistance (26) is calculated by the following manner:

$$\frac{\partial R}{\partial x_i} = Re\left\{\frac{\partial Z}{\partial x_i}\right\} \tag{39}$$

Now, it is necessary to calculate the differentiation of the electrical impedance (23) with respect to the design variables:

$$\frac{\partial Z}{\partial x_i} = \mathbf{\Phi}_{e1}^T \frac{\partial \mathbf{I}}{\partial x_i} = -i\omega \mathbf{\Phi}_{e1}^T \frac{\partial \mathbf{Q}_{e1}}{\partial x_i} \tag{40}$$

The derivative of the electrical charge vector $\mathbf{Q}_{e1}$ at the electrode is obtained by differentiating (21):

$$\frac{\partial \mathbf{Q}_{e1}}{\partial_{x_i}} = \underbrace{\begin{bmatrix} \frac{\partial \mathbf{K}^T_{\mathbf{u}\phi_{e1}}}{\partial x_i} & \frac{\partial \mathbf{K}^T_{\phi_f\phi_{e1}}}{\partial x_i} & \frac{\partial \mathbf{K}^T_{\phi_{e1}\phi_{e1}}}{\partial x_i} \end{bmatrix} \begin{Bmatrix} \mathbf{U} \\ \mathbf{\Phi}_f \\ \mathbf{\Phi}_{e1} \end{Bmatrix}}_{\frac{\partial \mathbf{Q}_{e1}}{\partial x_i}^A} + \underbrace{\begin{bmatrix} \mathbf{K}^T_{\mathbf{u}\phi_{e1}} & \mathbf{K}^T_{\phi_f\phi_{e1}} \end{bmatrix} \begin{Bmatrix} \frac{\partial \mathbf{U}}{\partial x_i} \\ \frac{\partial \mathbf{\Phi}_f}{\partial x_i} \end{Bmatrix}}_{\frac{\partial \mathbf{Q}_{e1}}{\partial x_i}^B} \tag{41}$$

Since $\mathbf{\Phi}_{e1}$ is constant (input electric potential), its differentiation with respect to the design variables is equal to 0, and it has been omitted in (41). The derivative of $\mathbf{U}$ and $\mathbf{\Phi}_f$ are calculated by differentiating 20:

$$\begin{Bmatrix} \frac{\partial \mathbf{U}}{\partial x_i} \\ \frac{\partial \mathbf{\Phi}_f}{\partial x_i} \end{Bmatrix} = -\begin{bmatrix} -\omega^2\mathbf{M}_{\mathbf{uu}} + \mathbf{K}_{\mathbf{uu}} & \mathbf{K}_{\mathbf{u}\phi_f} \\ \mathbf{K}^T_{\mathbf{u}\phi_f} & \mathbf{K}_{\phi_f\phi_f} \end{bmatrix}^{-1} \begin{bmatrix} \frac{\partial \mathbf{K}_{\mathbf{uu}}}{\partial x_i} & \frac{\partial \mathbf{K}_{\mathbf{u}\phi_f}}{\partial x_i} & \frac{\partial \mathbf{K}_{\mathbf{u}\phi_{e1}}}{\partial x_i} \\ \frac{\partial \mathbf{K}\mathbf{u}\phi_f{}^T}{\partial x_i} & \frac{\partial \mathbf{K}_{\phi_f\phi_f}}{\partial x_i} & \frac{\partial \mathbf{K}_{\phi_f\phi_{e1}}}{\partial x_i} \end{bmatrix} \begin{Bmatrix} \mathbf{U} \\ \mathbf{\Phi}_f \\ \mathbf{\Phi}_{e1} \end{Bmatrix} \tag{42}$$

In (42), it is necessary to invert the matrix in parenthesis. Given that this matrix depends on the frequency $\omega$, this inversion must be calculated for all frequency band, i.e., $n_f$ inversions. The matrix inversion is complicated and very slow, which makes the sensitivity calculation impracticable due to many inversions. To remedy that, it is possible to manipulate the involved matrices by using the adjoint method. By substituting (42) in (41), $\frac{\partial \mathbf{Q}_{e1}}{\partial x}^B$ can be written as:

$$\frac{\partial \mathbf{Q}_{e1}}{\partial x_i}^B = -\mathbf{K}_1\mathbf{K}_2^{-1}\mathbf{K}_3 \begin{Bmatrix} \mathbf{U} \\ \mathbf{\Phi}_f \\ \mathbf{\Phi}_{e1} \end{Bmatrix} \tag{43}$$

where

$$\mathbf{K}_1 = \begin{bmatrix} \mathbf{K}^T_{\mathbf{u}\phi_{e1}} & \mathbf{K}^T_{\phi_f\phi e1} \end{bmatrix} \tag{44}$$

$$\mathbf{K}_2 = \begin{bmatrix} -\omega^2\mathbf{M}_{\mathbf{uu}} + \mathbf{K}_{\mathbf{uu}} & \mathbf{K}_{\mathbf{u}\phi_f} \\ \mathbf{K}^T_{\mathbf{u}\phi_f} & \mathbf{K}_{\phi_f\phi_f} \end{bmatrix} \tag{45}$$

$$\mathbf{K}_3 = \begin{bmatrix} \frac{\partial \mathbf{K}_{\mathbf{uu}}}{\partial x_i} & \frac{\partial \mathbf{K}_{\mathbf{u}\phi_f}}{\partial x_i} & \frac{\partial \mathbf{K}_{\mathbf{u}\phi_{e1}}}{\partial x_i} \\ \frac{\partial \mathbf{K}\mathbf{u}\phi_f{}^T}{\partial x_i} & \frac{\partial \mathbf{K}_{\phi_f\phi_f}}{\partial x_i} & \frac{\partial \mathbf{K}_{\phi_f\phi_{e1}}}{\partial x_i} \end{bmatrix} \tag{46}$$

In (43), it is possible to modify the sequence of matrices $\mathbf{K}_1$ and $\mathbf{K}_2$:

$$\frac{\partial \mathbf{Q}_{e1}}{\partial x_i}^B = -\left(\left(\mathbf{K}_2^{-1}\right)^* \mathbf{K}_1^*\right)^* \mathbf{K}_3 \begin{Bmatrix} \mathbf{U} \\ \mathbf{\Phi}_f \\ \mathbf{\Phi}_{e1} \end{Bmatrix} \tag{47}$$

where * denotes the conjugate transpose of the matrix. Considering that $\left(\mathbf{K}_2^{-1}\right)^* = (\mathbf{K}_2^*)^{-1}$, (47) can be rewritten as:

$$\frac{\partial \mathbf{Q}_{e1}}{\partial x_i}^B = -\mathbf{K}^*_{adj}\mathbf{K}_3 \begin{Bmatrix} \mathbf{U} \\ \mathbf{\Phi}_f \\ \mathbf{\Phi}_{e1} \end{Bmatrix} \tag{48}$$

where $\mathbf{K}_{adj}$ is obtained by solving the following linear system of equations:

$$\mathbf{K}_2^*\mathbf{K}_{adj} = \mathbf{K}_1^* \tag{49}$$

The next step is to differentiate the components of the stiffness matrix. Notice that in (46), the derivative of the stiffness matrix is separated by degrees of freedom $\phi_l$ and $\phi_{e1}$. However, it is possible to calculate the differentiation of (11), (12), and (13), and then separate them into the mentioned degrees of freedom. Thus,

$$\frac{\partial \mathbf{K_{uu}}^e}{\partial x_i} = 2\pi \int_{-1}^{1}\int_{-1}^{1} \mathbf{B_u}^T \frac{\partial \mathbf{c}}{\partial x_i} \mathbf{B_u} r |\mathbf{J}| d\eta d\xi \tag{50}$$

$$\frac{\partial \mathbf{K}^e_{\mathbf{u}\phi}}{\partial x_i} = 2\pi \int_{-1}^{1}\int_{-1}^{1} \mathbf{B_u}^T \frac{\partial \mathbf{e}}{\partial x_i} \mathbf{B}_\phi r |\mathbf{J}| d\eta d\xi \tag{51}$$

$$\frac{\partial \mathbf{K}^e_{\phi\phi}}{\partial x_i} = 2\pi \int_{-1}^{1}\int_{-1}^{1} \mathbf{B}_\phi^T \frac{\partial \boldsymbol{\epsilon}}{\partial x_i} \mathbf{B}_\phi r |\mathbf{J}| d\eta d\xi \tag{52}$$

$$\tag{53}$$

which means that the differentiation of the stiffness matrix depends on the differentiation of the elastic $\mathbf{c}$, piezoelectric $\mathbf{e}$, and dielectric $\boldsymbol{\epsilon}$ property matrices with respect to the design variables. By the chain rule, the matrices properties must be first differentiated with respect to the material properties, and then the material properties are differentiated with respect to the design variables. The differentiation of (6), (7), and (8) with respect to each material property is equal to 1 only in the position where each property appears and zeros in the remainder positions. For instance, by differentiating the elastic property matrix of (6) with respect to $c_{11}$ and $\bar{c}_{11}$ is equal to:

$$\frac{\partial \mathbf{c}}{\partial c_{11}} = \begin{bmatrix} 1 & 0 & 0 & 0 \\ 0 & 1 & 0 & 0 \\ 0 & 0 & 0 & 0 \\ 0 & 0 & 0 & 0 \end{bmatrix} \quad ; \quad \frac{\partial \mathbf{c}}{\partial \bar{c}_{11}} = \begin{bmatrix} 1i & 0 & 0 & 0 \\ 0 & 1i & 0 & 0 \\ 0 & 0 & 0 & 0 \\ 0 & 0 & 0 & 0 \end{bmatrix} \tag{54}$$

Analogous procedure must be done for all real and imaginary properties. Finally, the differentiation of the material properties with respect to the design variables can be calculated by differentiating the properties in table 3, which yields to:

**Table 4.** Differentiation of the material properties with respect to the design variables.

| | |
|---|---|
| $\partial c_{11}/\partial x_1 = 10^4$ | $\partial \bar{c}_{11}/\partial x_{11} = 10^2$ |
| $\partial c_{12}/\partial x_2 = 10^4$ | $\partial \bar{c}_{12}/\partial x_{12} = 10^2$ |
| $\partial c_{13}/\partial x_3 = 10^4$ | $\partial \bar{c}_{13}/\partial x_{13} = 10^2$ |
| $\partial c_{33}/\partial x_4 = 10^4$ | $\partial \bar{c}_{33}/\partial x_{14} = 10^2$ |
| $\partial c_{44}/\partial x_5 = 10^4$ | $\partial \bar{c}_{44}/\partial x_{15} = 10^2$ |
| $\partial e_{31}/\partial x_6 = 10^3$ | $\partial \bar{e}_{31}/\partial x_{16} = 10$ |
| $\partial e_{15}/\partial x_7 = 10^3$ | $\partial \bar{e}_{15}/\partial x_{17} = 10$ |
| $\partial e_{33}/\partial x_8 = 10^3$ | $\partial \bar{e}_{33}/\partial x_{18} = 10$ |
| $\partial \epsilon_{11}/\partial x_9 = 10^2\epsilon_0$ | $\partial \bar{\epsilon}_{11}/\partial x_{19} = \epsilon_0$ |
| $\partial \epsilon_{33}/\partial x_{10} = 10^2\epsilon_0$ | $\partial \bar{\epsilon}_{33}/\partial x_{20} = \epsilon_0$ |

## 4. Conditions to Guarantee the Convergence

The convergence of the optimization problem is achieved when the absolute difference between the objective function values of subsequent iterations $(itt-1, itt)$ is lesser than a predefined convergence tolerance $(\delta_{conv})$.

$$\text{Condition 1: } |\mathfrak{F}^{itt} - \mathfrak{F}^{itt-1}| < \delta_{conv} \tag{55}$$

where $\delta_{conv} = 10^{-10}$ is proposed to guarantee that the objective function and the design variables are not changing anymore. If (55) is satisfied, than the optimization process stops, and a local minimum has been achieved. However, the problem may converge to an undesired local minimum, which can be identified graphically or numerically. Graphical identification makes the method non-systematic and is not used in this work. The numerical identification of an optimal or an undesired local minima can be measured by the objective function value $\mathfrak{F}$ of (30) and by defining an objective function tolerance $(\delta_{obj})$. Thus, another condition is proposed:

$$\text{Condition 2: } \mathfrak{F}^{itt} < \delta_{obj} \tag{56}$$

However, there is not a specific value for $\delta_{obj}$ that excludes all undesired local minima. Based on the tests performed in this work, it is proposed to use $\delta_{obj} = 10$. However, this value can be different for different materials. If (56) is never satisfied, than $\delta_{obj}$ can be raised to attend another specific problem.

Thus, if (55) and (56) are satisfied, then the optimal solution has been achieved and the full complex piezoelectric properties have been obtained. If only (55) is satisfied, than the solution is trapped in an undesired local minimum.

It has been noticed that the initial values of the design variables play a very important role in the success of the method. An improper choice of these values makes the solution to get trapped in an undesired local minimum. However, a priori it is not possible to predict whether these values will result in a good or a bad solution, and there is no rule to define the initial design variables which results in a good solution. This problem can be avoided in two ways, one more physical by performing a sensitivity analysis and a rough approach algorithm, as described in [10], or the other by restarting the design variables with random values if the problem does not converge. Due to the simulation speed improvement by the use of MMA and the 8-noded element, the choice of restarting the design variables with different values is possible in practice. Hence, if condition in (55) is satisfied, but condition in (56) is not, then the design variables are redefined randomly. It must be noticed that the MMA algorithm also needs to be restarted ($a_i^l = 0$, $a_i^u = 1$).

The initial design variable values representing the real part of the material properties are defined based on the properties given by the manufacturer of the piezoelectric material. In the case this information does not exist, the properties of a similar material can be used, or the method presented in [10, 14] can be used to obtain these initial values for the real part of the model. For instance, considering the material properties of the Pz27 provided by the manufacturer, and the scaling presented

in table 3, the initial design variables (represented by a tilde $\sim$) of the real part of the model are defined in table 5.

**Table 5.** Initial values of the design variables based on the properties provided by the manufacturer.

| $\tilde{x}_1$ | $\tilde{x}_2$ | $\tilde{x}_3$ | $\tilde{x}_4$ | $\tilde{x}_5$ | $\tilde{x}_6$ | $\tilde{x}_7$ | $\tilde{x}_8$ | $\tilde{x}_9$ | $\tilde{x}_{10}$ |
|---|---|---|---|---|---|---|---|---|---|
| 14.7 | 10.5 | 9.37 | 11.3 | 2.3 | 3.09 | 10.67 | 12.4 | 11.3 | 9.14 |

If the optimization loop restarts, then the initial design variables for the new loop must be modified, otherwise the same solution is obtained. Thus, it is proposed to use random values inside a range of $\pm 20\%$ of $\tilde{x}$ every time the loop restarts. To obtain random values, the "*rand*" function from MatLab is used as:

$$x_i = r_i^{min} + rand(1)\left(r_i^{max} - r_i^{min}\right), \quad i = 1, \ldots, 10 \tag{57}$$

where

$$\left.\begin{array}{l} r_i^{min} = 0.8\tilde{x}_i \\ r_i^{max} = 1.2\tilde{x}_i \end{array}\right\} \quad i = 1, \ldots, 10 \tag{58}$$

and $rand(1)$ creates a random value between 0 and 1.

In the case of the imaginary part of the model, there is no particular rule to define the initial values. Based on the results presented by [14], it is proposed to define the initial design variables of the imaginary part of the model as:

$$\tilde{x}_{11,\ldots,16} = \tilde{x}_{1,\ldots,6} \text{ and } \tilde{x}_{17,\ldots,20} = -\tilde{x}_{7,\ldots,10} \tag{59}$$

This rule also applies if the loop restarts. However, there is another issue that needs to be handled. Depending on the values of the imaginary properties during the optimization, there is the possibility that the electrical conductance and resistance assume negative values, which is numerically possible, however, physically unfeasible. One way to handle negative values of conductance and resistance is to use constraints in the optimization algorithm. For instance, the constraints can be formulated as:

$$\text{Condition 3: } G_j \geq 0 \text{ and } R_j \geq 0, \ \forall j = 1, \ldots, n_f \tag{60}$$

However, the MMA algorithm has a relaxed way to deal constraints, which means that they can be violated during the process to prevent local minima, even though they must be satisfied at the final step of the optimization. Because of the $\log_{10}$ function used in the objective function, the conductance and the resistance cannot be negative at anytime. Thus, another way to deal with this issue is to restart the optimization loop if the condition in (60) is violated. Thus, all three conditions in (55), (56), and (60) must be satisfied to guarantee that a satisfactory solution has been achieved.

Another approach used to improve the simulation speed is to divide the method in two steps: preliminary and refinement steps. The preliminary step is considered while (56) is not satisfied. The domain is discretized with a coarse mesh in order to achieve a solution close to the optimal solution. According to the mesh convergence test

presented in section 2.1, a 20x2 mesh discretization can be used in the preliminary step, although not accurate, it is 6 times faster than the 50x5 mesh discretization. Once (56) is satisfied, the refinement step is considered, and the mesh is refined so that the optimal solution is achieved and more accurate values of the design variables are obtained. The discretization used in this step is equal to 50x5 elements, which is shown (in section 2.4) to be as accurate as more refined meshes and up to sixteen times faster (regarding processing times).

## 5. Method Validation with Numerical Results

In this section, the validation of the method is presented. To validate the method the full piezoelectric material properties obtained in section 6 are used to build a FEM model of the piezoceramic. Then, the electrical response of this numerical model is calculated and it is used as a reference in the proposed method. The reference curves have been obtained by using a mesh equal to 200x20 elements, which is different and more refined than the meshes used in the proposed method to avoid "inverse crime". The optimized properties are supposed to be slightly different from the reference properties only because of the discretization difference, and not because of geometry or material imperfections. The diameter and thickness of the piezoceramic disc are equal to $d = 20$ mm and $h = 2$ mm, respectively, and the material density is equal to $\rho = 7707$ kg/m$^3$.

According to (34), the minimum and maximum boundaries of the design variables must be defined. For this example, the following boundaries are defined:

$$\begin{array}{rcll} 0 & \leq x_i \leq & 30 & \text{for } i = 1, \ldots, 10 \\ \text{-}300 & \leq x_i \leq & 300 & \text{for } i = 11, \ldots, 20 \end{array} \tag{61}$$

The maximum value for the real variables have been defined based on the existing material properties. On the other hand, the limits for the imaginary variables have been established empirically, based on tests performed in this work. These values works fine for soft piezoelectric ceramics, such as Pz27. However, these limits may be properly modified to meet other material conditions.

The initial design variables representing the real part of the properties are listed in table 5, and the initial design variables representing the imaginary part are calculated by (59). The initial objective function value is equal to $\mathfrak{F} = 572$.

Figure 6 presents the objective function evolution through the optimization process. The final objective function value is equal to $\mathfrak{F} = 1.4 \times 10^{-3}$. The design variables have been redefined 6 times before the optimized solution is achieved. Peaks 3 and 4 indicate that condition 3 has been violated, while peaks 1, 2, 5, and 6 indicate that the solution has converged to an undesired local minima. The hole process required 352 iterations and took only 20 minutes and 53 seconds (by using the PC configuration mentioned in section 1).

Figure 7 shows the comparison between the numerical reference and optimized electrical impedance curves at the end of the optimization process. It can be noticed

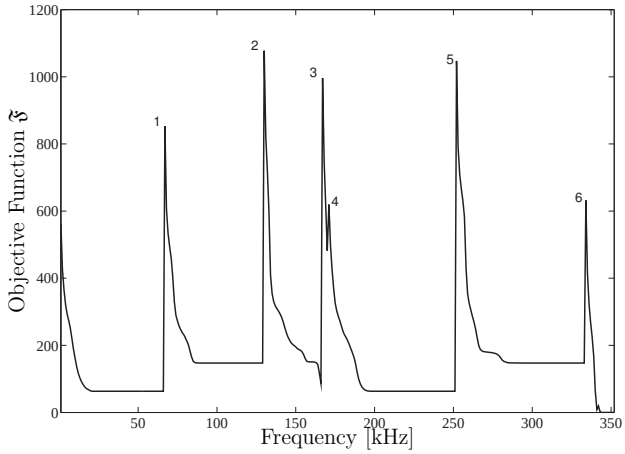


**Figure 6.** Convergence graph of the objective function evolution.

that the electrical response for the optimized properties fits precisely to the reference electrical response, even with the mesh discretization difference.

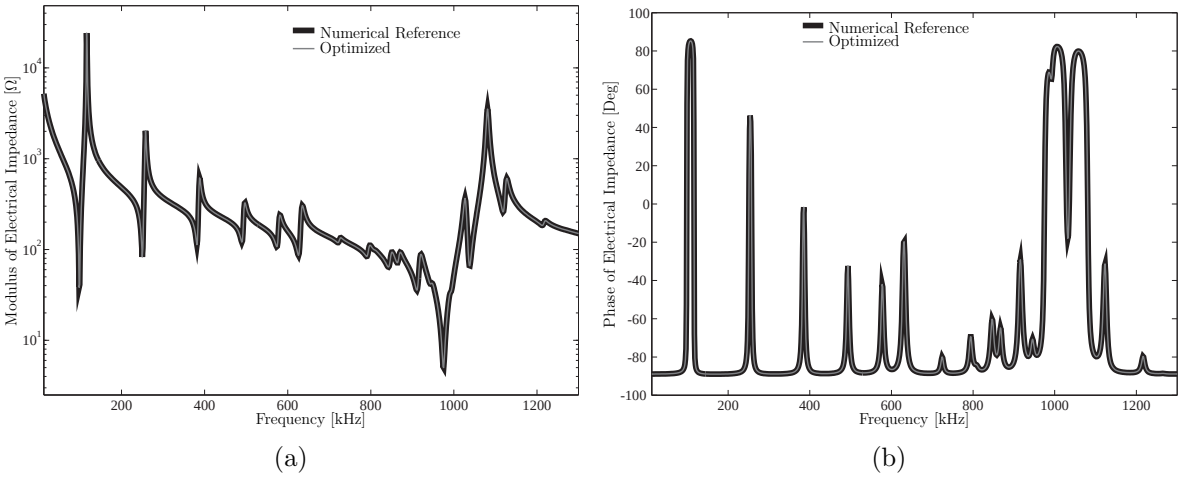


**Figure 7.** Numerical reference and optimized electrical impedance curves: (a) modulus; and (b) phase.

Table 6 lists the full piezoelectric complex properties of the numerical reference and the optimized cases. The percentage differences between both of them are presented, which are calculated as $100|x_i^{ref} - x_i^{opt}|/|x_i^{ref}|$. Precise solutions are obtained for the real part of the properties, where the only non-zero, but very small, difference is found for $\epsilon_{11}$. In the case of the imaginary properties, most of them show precise solutions, except for $\bar{c}_{11}$, $\bar{e}_{15}$, and $\bar{\epsilon}_{11}$ which show a very small difference from the reference properties. However, these small differences can be neglected, since the absolute difference is very small when compared to the real properties.

**Table 6.** Validation example. Comparison of the reference properties with the optimized properties.

| | Ref. | Opt. | Diff. % | | Ref. | Opt. | Diff. % |
|---|---|---|---|---|---|---|---|
| $c_{11}$ [GPa] | 117.7 | 117.7 | 0.0 | $\bar{c}_{11}$ [GPa] | 0.42 | 0.43 | 2.4 |
| $c_{12}$ [GPa] | 73.7 | 73.7 | 0.0 | $\bar{c}_{12}$ [GPa] | -0.26 | -0.26 | 0.0 |
| $c_{13}$ [GPa] | 73.3 | 73.3 | 0.0 | $\bar{c}_{13}$ [GPa] | -0.14 | -0.14 | 0.0 |
| $c_{33}$ [GPa] | 109.7 | 109.7 | 0.0 | $\bar{c}_{33}$ [GPa] | 0.40 | 0.40 | 0.0 |
| $c_{44}$ [GPa] | 20.3 | 20.3 | 0.0 | $\bar{c}_{44}$ [GPa] | 0.41 | 0.41 | 0.0 |
| $e_{31}$ [C/m$^2$] | -5.2 | -5.2 | 0.0 | $\bar{e}_{31}$ [C/m$^2$] | 0.035 | 0.035 | 0.0 |
| $e_{15}$ [C/m$^2$] | 11.6 | 11.6 | 0.0 | $\bar{e}_{15}$ [C/m$^2$] | 0.035 | 0.032 | 8.6 |
| $e_{33}$ [C/m$^2$] | 16.0 | 16.0 | 0.0 | $\bar{e}_{33}$ [C/m$^2$] | -0.079 | -0.079 | 0.0 |
| $\epsilon_{11}/\epsilon_0$ | 950 | 952 | 0.2 | $\bar{\epsilon}_{11}/\epsilon_0$ | 15.77 | 15.05 | 4.6 |
| $\epsilon_{33}/\epsilon_0$ | 815 | 815 | 0.0 | $\bar{\epsilon}_{33}/\epsilon_0$ | -10.68 | -10.68 | 0.0 |

## 6. Experimental Result

In this section, the proposed optimization method is applied to find the full piezoelectric complex properties of a Pz27 sample. The diameter and the thickness of this sample are equal to $d = 20$ mm and $h = 2.004$ mm. The material density is measured by using the Archimedes principle, and it is equal to $\rho = 7707$ kg/m$^3$. The experimental data used to calculate the electrical impedance, phase, conductance, and resistance have been acquired by an impedometer. The experimental electrical impedance and phase curves are shown in figure 9 as the thick black curve.

The same initial design variables used in section 5 are used in this example. The design variables limits are also the same as used in the numerical validation example. The initial objective function value is equal to $\mathfrak{F} = 572$.

Figure 8 presents the evolution of the objective function through the optimization process, where the 9 peaks denote that the design variables have been redefined before a satisfactory solution is achieved. The peaks 1 and 9 indicate that condition 1 has been satisfied and condition 2 has not, and thus, the design variables have been redefined. The other peaks indicate a violation of condition 3. The final objective function value is equal to $\mathfrak{F} = 3.18$, and the hole process required 273 iterations and took only 18 minutes and 21 seconds to run (by using the PC configuration mentioned in section 1). However, this performance cannot be always guaranteed because the design variables are redefined randomly.

Figure 9 shows the comparison between the experimental and optimized electrical impedance curves at the end of the optimization process. It can be seen that both curves are superposed for the hole bandwidth. However, some regions (indicated by the arrows) are not perfectly adjusted. This difference is mainly caused by the imperfections of the sample, for instance, parallelism of faces, porosity, etc., while the numerical model assumes an ideal sample.

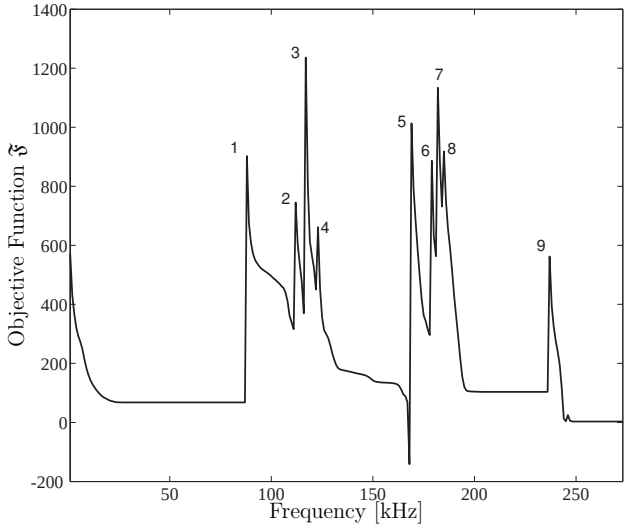


**Figure 8.** Convergence graph of the objective function evolution.

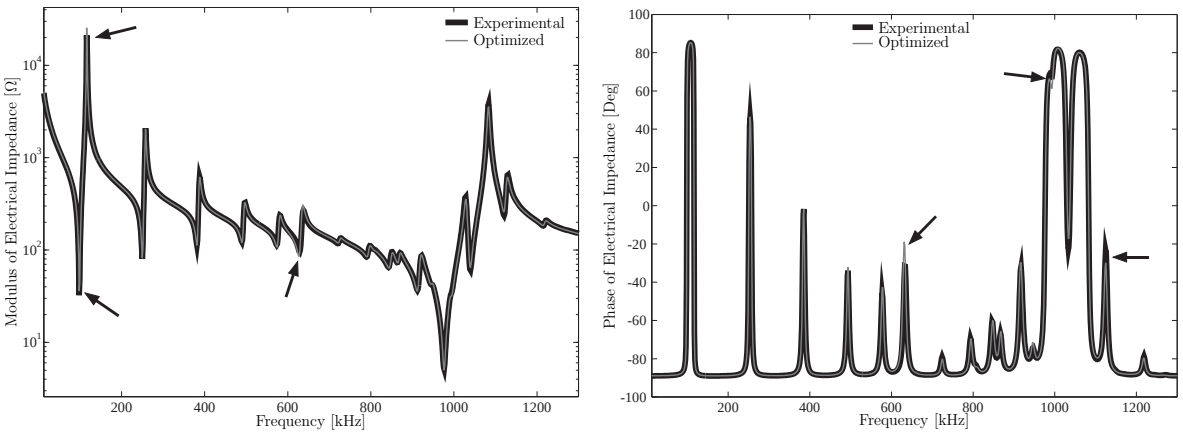


(a) (b)

**Figure 9.** Experimental and optimized electrical impedance curves: (a) modulus; and (b) phase.

Table 7 lists the full optimized piezoelectric complex properties of the sample used in this example. By comparing the optimized real properties with the manufacturer real properties (see table 7), it can be noticed a great difference for all values. Thus, by analyzing the graphs shown before, the optimized result obtained here can reproduce the experimental electrical response of the Pz27 sample, whereas the properties provided by the manufacturer cannot (see figure 1).

Because there is no exact properties to compare the presented results, the accuracy of the proposed method is evaluated by starting the process with random initial properties in the range of $\pm 20\%$ around the properties given in table 5 and by calculating the mean and the standard deviation of the optimized results. 100 tests have been performed in this accuracy evaluation. The maximum and minimum reset count are equal to 30 and 0, respectively, which corresponds to evaluation times equal to 44 and

**Table 7.** Experimental example. Full optimized piezoelectric complex properties of the Pz27 sample used in this example.

| | | | |
|---|---|---|---|
| $c_{11}$ [GPa] | 117.7 | $\bar{c}_{11}$ [GPa] | 0.42 |
| $c_{12}$ [GPa] | 73.7 | $\bar{c}_{12}$ [GPa] | -0.26 |
| $c_{13}$ [GPa] | 73.3 | $\bar{c}_{13}$ [GPa] | -0.14 |
| $c_{33}$ [GPa] | 109.7 | $\bar{c}_{33}$ [GPa] | 0.40 |
| $c_{44}$ [GPa] | 20.3 | $\bar{c}_{44}$ [GPa] | 0.41 |
| $e_{31}$ [C/m$^2$] | -5.2 | $\bar{e}_{31}$ [C/m$^2$] | 0.035 |
| $e_{15}$ [C/m$^2$] | 11.6 | $\bar{e}_{15}$ [C/m$^2$] | 0.035 |
| $e_{33}$ [C/m$^2$] | 16.0 | $\bar{e}_{33}$ [C/m$^2$] | -0.079 |
| $\epsilon_{11}/\epsilon_0$ | 950 | $\bar{\epsilon}_{11}/\epsilon_0$ | 15.77 |
| $\epsilon_{33}/\epsilon_0$ | 815 | $\bar{\epsilon}_{33}/\epsilon_0$ | -10.68 |

4 minutes, respectively. Table 8 shows the mean values of the optimized properties with the respective standard deviation. It can be seen that the standard deviations are very low compared to the mean values, which means that the proposed method is very accurate.

**Table 8.** Accuracy evaluation of the proposed method.

| | Mean | SD | | Mean | SD |
|---|---|---|---|---|---|
| $c_{11}$ [GPa] | 117.6 | $0.85\times10^{-6}$ | $\bar{c}_{11}$ [GPa] | 0.41 | $0.24\times10^{-6}$ |
| $c_{12}$ [GPa] | 73.7 | $0.12\times10^{-6}$ | $\bar{c}_{12}$ [GPa] | -0.27 | $0.46\times10^{-6}$ |
| $c_{13}$ [GPa] | 73.4 | $0.47\times10^{-6}$ | $\bar{c}_{13}$ [GPa] | -0.15 | $0.14\times10^{-6}$ |
| $c_{33}$ [GPa] | 110.2 | $0.25\times10^{-6}$ | $\bar{c}_{33}$ [GPa] | 0.40 | $0.06\times10^{-6}$ |
| $c_{44}$ [GPa] | 20.4 | $0.14\times10^{-6}$ | $\bar{c}_{44}$ [GPa] | 0.42 | $0.10\times10^{-6}$ |
| $e_{31}$ [C/m$^2$] | -5.2 | $0.05\times10^{-6}$ | $\bar{e}_{31}$ [C/m$^2$] | 0.034 | $0.02\times10^{-6}$ |
| $e_{15}$ [C/m$^2$] | 11.6 | $0.36\times10^{-6}$ | $\bar{e}_{15}$ [C/m$^2$] | 0.039 | $0.47\times10^{-6}$ |
| $e_{33}$ [C/m$^2$] | 16.1 | $0.31\times10^{-6}$ | $\bar{e}_{33}$ [C/m$^2$] | -0.079 | $0.01\times10^{-6}$ |
| $\epsilon_{11}/\epsilon_0$ | 961 | $80.7\times10^{-6}$ | $\bar{\epsilon}_{11}/\epsilon_0$ | 17.23 | $129.3\times10^{-6}$ |
| $\epsilon_{33}/\epsilon_0$ | 817 | $13.6\times10^{-6}$ | $\bar{\epsilon}_{33}/\epsilon_0$ | -10.71 | $1.59\times10^{-6}$ |

## 7. Concluding Remarks

This work presents a new efficient and systematic optimization method to find the full piezoelectric complex properties, by adjusting the real and imaginary parameters simultaneously and considering a wide frequency range. This method combines a higher-order axisymmetric plane element with a gradient-based optimization algorithm which results in lower computational time and very few user interaction. It has been proposed a restart approach to redefine the design variables if the solution is an undesired or unfeasible local minima.

The experimental result showed that the optimized properties can reproduce an electrical response very similar to the experimental curves. The method validation shows that in the case of a material that follows exactly the 6mm symmetry, the algorithm converges to the real solution. In this case, the convergence error can be numerically estimated. However, in theory, there is no way to determine the accuracy of and individual optimized property from the experimental result. The complete model can be experimentally evaluated by using mechanical magnitudes, for example a vibrometer to obtain the displacement field.

The method presented in this work has been applied only for soft piezoelectric ceramics, such as Pz27 and APC 850. However, only the results for the Pz27 are presented. Finally, as future works, it is proposed to extend the method to hard piezoceramics.

## 8. Acknowledgements

Kiyono thanks FAPESP (São Paulo Research Foundation) for the financial support during his post-doctoral (grants 2012/14576-9 and 2015/06334-3). Pérez also thanks FAPESP for the financial support during his visitant professor at the University of São Paulo and the uruguayan funding agencies ANII, CSIC, and PEDECIBA. Silva thanks the financial support of FAPESP and CNPq (National Council for Research and Development) under grant 304121/2013-4.

## References

[1] Catalogue ferroperm piezoceramics URL `https://ida.dk/node/73203/files/12915`
[2] Smits J G 1976 *Sonics and Ultrasonics, IEEE Transactions on* **23** 393–401
[3] Alemany C, Pardo L, Jimenez B, Carmona F, Mendiola J and Gonzalez A 1994 *Journal of Physics D: Applied Physics* **27** 148
[4] Sherrit S, Wiederick H D, Mukherjee B K and Sayer M 1997 *Journal of Physics d: applied physics* **30** 2354
[5] Joo H W, Lee C H, Rho J S and Jung H K 2003 *Ultrasonics, Ferroelectrics, and Frequency Control, IEEE Transactions on* **50** 965–971
[6] Pardo L, Algueró M and Brebøl K 2007 *Journal of Physics D: Applied Physics* **40** 2162
[7] Meeker T R 1996 *IEEE Transactions on Ultrasonics Ferroelectrics and Frequency Control* **43** 717–772
[8] Kaltenbacher B, Kaltenbacher M, Lerch R and Simkovics R 2000 Identification of material tensors for piezoceramic materials *Ultrasonics Symposium, 2000 IEEE* vol 2 (IEEE) pp 1033–1036
[9] Lahrner T, Kaltenbacher M, Kaltenbacher B, Lerch R and Leder E 2008 *Ultrasonics, Ferroelectrics, and Frequency Control, IEEE Transactions on* **55** 465–475
[10] Pérez N, Andrade M A B, Buiochi F and Adamowski J C 2010 *Ultrasonics, Ferroelectrics, and Frequency Control, IEEE Transactions on* **57** 2772–2783
[11] Holland R 1967 *Sonics and Ultrasonics, IEEE Transactions on* **14** 18–20
[12] Algueró M, Alemany C, Pardo L and González A M 2004 *Journal of the American Ceramic Society* **87** 209–215
[13] Sherrit S, Masys T J, Wiederick H D and Mukherjee B K 2011 *Ultrasonics, Ferroelectrics, and Frequency Control, IEEE Transactions on* **58** 1714–1720

[14] Pérez N, Carbonari R C, Andrade M A B, Buiochi F and Adamowski J C 2014 *Ultrasonics* **54** 1631–1641
[15] Svanberg K 1987 *International journal for numerical methods in engineering* **24** 359–373
[16] Ikeda T 1990 *Fundamentals of piezoelectricity.* (Oxford University Press, Oxford)
[17] Bathe K J 2006 *Finite element procedures* (Prentice Hall)
[18] Buiochi F, Pérez N and Adamowski J C 2014 *Comprehensive Materials Processing* vol 2 (Elsevier) chap 2.04 Ultrasonic Characterization of Anisotropic Materials